Chikungunya Virus RNA Secondary Structures Impact Defective Viral Genomes Production

Laura I LEVI *, Emily A Madden, Jeremy Boussier, Diana Erazo, Wes Sanders, Thomas Valley, Veronika Bernhauerová, Nathaniel J. J Moorman, Mark T Heise, Marco Vignuzzi

Posted Date: 15 July 2024

doi: 10.20944/preprints202407.1212.v1

Keywords: chikungunya virus; defective viral genomes; RNA secondary structure; SHAPE-MAP

Article

Chikungunya Virus RNA Secondary Structures Impact Defective Viral Genomes Production

Laura I. Levi [1,2,*], Emily A. Madden [3], Jeremy Boussier [1], Diana Erazo [1], Wes Sanders [3], Thomas Vallet [1], Veronika Bernhauerova [1], Nathaniel J. Moorman [3,4], Mark T. Heise [3,5] and Marco Vignuzzi [1,6]

[1] Institut Pasteur, Populations Virales et Pathogenèse, CNRS UMR 3569, CNRS, Paris 75015, France
[2] Université Paris Cité and Hôpital Saint-Louis and Lariboisière, INSERM U944, Paris, France
[3] Department of Microbiology and Immunology, UNC-Chapel Hill, USA
[4] Lineberger Comprehensive Cancer Center, UNC-Chapel Hill, USA
[5] Department of Genetics, UNC-Chapel Hill, USA
[6] A*STAR Infectious Diseases Labs (A*STAR ID Labs), Agency for Science, Technology and Research (A*STAR), 8A Biomedical Grove, Immunos #05-13, Singapore 138648, Singapore
* Correspondence: laura.levi@aphp.fr; Tel.:01 42 49 90 64

Abstract: Chikungunya virus (CHIKV) is a mosquito borne RNA virus that poses an emerging threat to humans. As other RNA viruses, CHIKV encodes an error-prone RNA polymerase which, in addition to full-length genomes, gives rise to truncated, non-functional genomes coined defective viral genomes (DVGs). DVGs have been in-tensively studied in the context of therapy, as they can inhibit viral replication and dissemination in their hosts. In this work, we interrogate the influence of viral RNA secondary structures on the production of CHIKV DVGs. We experimentally map RNA secondary structures of CHIKV genome using selective 2′-hydroxyl acylation analyzed by primer extension and mutational profiling (SHAPE-MaP), which couples chemical labelling with next-generation sequencing. We correlate the inferred secondary struc-ture with preferred deletion sites of CHIKV DVGs. We document an increased proba-bility of DVG generation with truncations at unpaired nucleotides within the second-ary structure. We then generated a CHIKV mutant bearing synonymous changes at the nucleotide level to disrupt existing RNA secondary structure (CHIKV-D2S). We show that CHIKV-D2S presents altered DVG generation compared to wild-type virus, corre-lating with its change in RNA secondary structure obtained by SHAPE-MaP. Our work thus demonstrates that RNA secondary structure impacts CHIKV DVG production during replication.

Keywords: chikungunya virus; defective viral genome; RNA secondary structure; SHAPE-MaP.

1. Introduction

Chikungunya virus (CHIKV), which belongs to the alphavirus genus and Togaviridae family, is a positive strand RNA virus. During its acute phase, CHIKV is responsible for a dengue-like syndrome associating brutal fever with symptoms such as severe joint pain or rash (Borgherini et al. 2007; Suhrbier et al. 2012; Bouquillard et al. 2018; Levi et Vignuzzi 2019). CHIKV infection can lead to year-long polyarthralgia which incapacitates patients and strongly impacts their quality of life (Suhrbier et al. 2012; Levi et Vignuzzi 2019; Couturier et al. 2012; Borgherini et al. 2008). CHIKV has been responsible for two worldwide epidemics since the beginning of the 21st century affecting 60 countries and causing close to 8 million cases altogether (Chretien et al. 2007; Vignuzzi et Higgs 2017; Levi et Vignuzzi 2019). As most RNA viruses, the error-prone replication of CHIKV in infected cells leads to the production of defective viral genomes (DVGs) (Poirier et al. 2018; Levi et al. 2021), which represent mutated, truncated or rearranged genomes. DVGs are unable to complete a full viral cycle but have been documented to influence viral replication and the activation of the immune system (Vignuzzi et López 2019; Rezelj, Levi, et Vignuzzi 2018; Monroe et Schlesinger 1984). Notably, they

 doi:10.20944/preprints202407.1212.v1

are strong inducers of pro-inflammatory cytokines, including type-I interferons, as documented during syncytial respiratory virus and influenza virus infections in animal models and patients (Marcus et Sekellick 1977; Sun et al. 2015; Vasilijevic et al. 2017; Easton et al. 2011). Work on arboviruses confirmed that this effect on innate immunity also exists in insects where DVGs from Sindbis, chikungunya and Zika viruses can modulate antiviral immunity (Poirier et al. 2018), and block viral dissemination and transmission in their mosquito vector (Levi et al. 2021; Rezelj et al. 2021). Truncated DVGs are hypothesized to arise via non-homologous recombination occurring during viral replication (Rezelj, Levi, et Vignuzzi 2018; Wang et al. 2022), a mechanism by which the viral error prone RNA-dependent RNA-polymerase (RdRp) detaches from its genome template at a specific position (hereafter referred to as "start breakpoint") and reattach to another position further along in the genome ("stop breakpoint"). The DVG arising from such an event will be truncated for the portion of genome between the start and stop breakpoints. While the existence of DVGs have been documented in CHIKV infection (Levi et al. 2021), the factors influencing their production are currently unknown.

A key parameter that influences recombination by viral polymerases is the existence of secondary and tertiary structures in viral RNA, generated by RNA folding on itself (Wang et al. 2022). These structures are essential for the viral life cycle as they are involved in replication and packaging (Nicholson et White 2015; Rausch et al. 2017) via the presence of local secondary RNA structure (such as hairpins or stem loops) and long-range interactions (Nicholson et White 2015; 2014). For example, four stem-loops in the 5'-UTR and start of nSP1 of the CHIKV genome are key for positive and negative strand RNA synthesis (Kutchko et al. 2018). Several studies link RNA secondary structure to homologous copy-choice recombination events, notably in human immunodeficiency virus (HIV) (Galetto et al. 2004; Moumen et al. 2003; Simon-Loriere et al. 2010), brome mosaic virus (Figlerowicz 2000), the poliovirus Sabin strain (Dedepsidis et al. 2010) and hepatitis delta virus (Chao et al. 2017). By this mechanism, when replicating the viral genome, the RdRp drops off the RNA template it started copying and reattaches to a second RNA template, giving rise to a hybrid RNA molecule. Because it detaches and reattaches at the same position on the RNA, the recombination is called homologous, and gives rise to a hybrid full-length RNA that is still infectious. Overall, the existence of secondary RNA structures is thought to shape the homologous recombination hotspots in the viral genome. Yet only a few studies have examined how the link between secondary RNA structures and non-homologous recombination might affect DVG formation. In at least one example, for Cymbidium ringspot virus, a highly base-paired region of a long DVG was thought to direct generation of a shorter DVG (Havelda et al. 1997).

RNA secondary structure analyses traditionally relied on thermodynamics-based, computer-aided structural predictions to determine the structure with the minimum free energy for folding, corresponding to the highest stability. These methods, however, must still be confirmed by experimental data. The technique selective 2'-hydroxyl acylation analyzed by primer extension and mutational profiling (SHAPE-MaP) is an improvement by producing experimentally informed RNA secondary structure models (Merino et al. 2005; Low et Weeks 2010; Wilkinson et al. 2006). SHAPE-MaP relies on selectively acetylating unpaired nucleotides, i.e. bases that are not involved in RNA secondary structures. The acetylated nucleotides are then identified as mutations by next generation sequencing (Siegfried et al. 2014). From the mutation data, each nucleotide position is assigned a SHAPE reactivity value: a high value if the nucleotide is paired; low, if the nucleotide is more likely unpaired. SHAPE-MaP can thus construct an experimentally-driven quantitative map of RNA secondary structure, which depicts the probability of a given nucleotide to be involved in RNA secondary structures. SHAPE-MaP was used to decipher the full secondary structure at a single-nucleotide level of several alphavirus RNA genomes, including Sindbis virus (SINV) (Kutchko et al. 2018), Venezuelan equine encephalitis virus (VEEV) (Kutchko et al. 2018), and more recently CHIKV (Madden et al. 2020).

In this work, we exploit the SHAPE-MaP of CHIKV genome to interrogate the influence of RNA secondary structures on non-homologous recombination events leading to DVG generation. We show that, in infected mammalian cells, the higher the probability for a given nucleotide to be

 doi:10.20944/preprints202407.1212.v1

unpaired, the higher the probability for it to be a DVG breakpoint. To experimentally verify this correlation, we generate a CHIKV mutant, termed CHIKV D2S for "disrupted secondary structures", which carries 76 synonymous mutations that abolish mapped RNA secondary structures in the first half of CHIKV genome. We observe that, although CHIKV D2S generates DVGs from the same genomic regions as wild-type (WT) CHIKV, DVGs arising from D2S replication are more diverse in terms of sequences and display a decreased accuracy of breakpoint position. The differences between CHIKV WT and D2S were more important in the region of the genome which was disrupted for secondary structure compared to the undisrupted region. Importantly, we could correlate the nature of the DVGs produced by the D2S mutant to its RNA genomic structure determined by SHAPE-MaP, directly implicating RNA secondary structures in the regulation of non-homologous recombination and DVG generation.

2. Materials and Methods

2.1. Cells and Virus

Vero and BHK cells were maintained in Dulbecco's modified Eagle's medium (DMEM), supplemented with 10% fetal calf serum (FCS; Gibco), 1% non-essential amino-acid (NEAA; Gibco) and 1% penicillin/streptomycin (P/S Thermo Fisher) in a humidified atmosphere at 37° C with 5% CO2.

The viral stocks were generated from chikungunya virus (CHIKV) infectious clones derived from the Caribbean strain, Asian genotype (described in Stapleford et al. (Stapleford et al. 2016)) or the disrupted secondary structure (D2S) mutant derived from it (see below). Plasmids were linearized with Not I enzyme (Thermo Fisher) and in vitro transcripted with SP6 mMESSAGE mMACHINE kit (Invitrogen). RNA from in vitro transcription (IVT) was then transfected in BHK cells using lipofectamin 2000 (Invitrogen) and passaged once in Vero cells. The stocks were titered and kept at -80°C before use. For D2S, the stocks were RNA extracted and Sanger sequenced to confirm the absence of reversion.

2.2. Cloning Selected Disrupted Secondary Structure (D2S) Mutant

Three regions of the original Caribbean CHIKV clone were mutated using the program CodonShuffle with the dn231 algorithm(Jorge, Mills, et Lauring 2015) in order to generated maximum secondary structure disruption with minimum change in codon usage.

Five 154 to 214 nucleotide-long double-stranded DNA (gBlocks® Gene Fragments) carrying the wanted mutations (Table S1) were ordered from IDT. Gene fragments were amplified by PCR using Q5 DNA polymerase (NEB). They were cloned into WT CHIKV Carib plasmid one after the other, amplifying the CHIKV Carib vector around the region to modify using Q5 DNA polymerase (NEB); list of primers used is available in Table S2. After DpnI (Thermo Fisher) treatment and gel purification (Macherey Nagel PCR and gel purification kit) of the vector, insert and vector were fused together with In-Fusion reagent (Takara Bio Reagent) following manufacturer's instructions, 2.5 µl was transformed in XL10-Gold extra competent cells (Stratagene). Colonies were grown in LB medium with ampicillin, to perform minipreps (NucleoSpin plasmid, Macherey Nagel) that were Sanger sequenced to confirm they carried the mutations expected.

2.3. Plaque Assay

Viral titration was performed on confluent Vero cells plated in 24-well plates, one day before infection. Ten-fold dilutions were done in DMEM alone and transferred onto Vero cells. After allowing infection for one hour, DMEM with 2% FCS, 1% P/S, 1% NEAA and 0,8% agarose was added on top of cells. Three days post infection, Vero cells were fixed with 4% formalin (Sigma), and plaques were manually counted after staining them with 0,2% crystal violet (Sigma).

 doi:10.20944/preprints202407.1212.v1

2.4. Viral Passages

Vero cells were seeded in 24-well plates to reach approximately 80% the next day. For passage 1, the viral stock was diluted in PBS to obtain a multiplicity of infection (MOI) of 5. After removing the cell culture medium, cells were incubated with the viral solution at 37°C for 1 hour. Following virus adsorption, the inoculum was removed and replaced with 600 µL of the appropriate cell culture medium containing 2% FCS. At 48–72 hours post infection, supernatant was harvested and clarified by centrifugation (12 000 x g, 5 min). The following passages were performed blindly, using 300 µl of the clarified supernatant from previous passage to infect naïve cells followed by the same procedure. A total of 8 passages were performed. Each passage was titered by plaque assay. Six replicates were performed per virus.

2.5. Growth Curves

Vero cells were seeded in 24 well-plates 24 hour prior to infection to reach 80% of confluence the next day. Virus stock was diluted in PBS to reach the wanted MOI (0,01 or 1) and incubated on cells. After on hour, virus was removed and cells were washed three times with PBS. Fresh medium supplemented with 2 FBS was added. At each time point, 50 ul of medium was harvested (kept at -80°) and replace by 50 µl of fresh medium. All samples were titered together by plaque assay. Both growth curves were realized in triplicates.

2.6. Deep-Sequencing

RNA of 100 µL of each sample was extracted using ZR-96 Viral RNA kit (Zymo) following the manufacturer's protocol, and eluted in 20 µL nuclease-free water. RNA library was produced with NEBNext Ultra II RNA Library kit (Illumina) using Multiplex oligos (Illumina). Libraries were quantified using the Quant-iT DNA assay kit (Thermo Fisher Scientific) and diluted to 1 nM prior to sequencing on a NextSeq sequencer (Illumina) with a NextSeq 500 Mid Output kit v2 (Illumina) (151 cycles).

2.7. SHAPE-MaP of WT and D2S CHIKV RNA

For determination of CHIKV secondary structure in Vero cells, the viral stock of WT or D2S mutant was passaged once in fresh Vero cells seeded in a T150 flask. Supernatants were harvested and viral RNA were extracted from sucrose-purified virions and analyzed as described before (Madden et al. 2020).

2.9. Data Analysis

2.9.1. Alignment and Identification of DVGs

BBTools suit was used to analyze the sequencing output (Bushnell B. - sourceforge.net/projects/bbmap/). BBDuk allowed us to trim for low-quality bases and adaptors fastq files generated from sample sequencing. Then, they were aligned to CHIKV reference sequence (Carib - GenBank accession no. LN898104.1, IOL - GenBank accession no. AM258994) using BBMap. To visualize the data, heatmaps of the deletion score of each nucleotide positions were generated using R. Specifically, scores were computed as the sum of the number of reads per million reads (RPM) supporting the deletion of a specific nucleotide position. For plotting start/stop breakpoints on R, deletions with lengths below 10 nucleotides were discarded.

2.9.2. Correlation between DVG Nucleotide Allele Frequency and SHAPE Reactivity

From the list of deletion generated from deep sequencing data as described above, we selected all deletions of 10 or more nucleotides. Breakpoints in the 3'UTR (i.e. after nucleotide 11302) were excluded, since SHAPE MaP is less accurate in that region because of sequence repeats (Marinus et al. 2021). From this list, we broke down the data by start and stop positions and associated allele

 doi:10.20944/preprints202407.1212.v1

frequency (in reads per million). Positions that were both start and stop positions were pooled separately and their associated allele frequency in reads per million were summed up. Next, we matched the raw SHAPE reactivity value to each position, and calculated a Pearson correlation coefficient.

2.9.3. Comparison of the SHAPE Reactivity of Nucleotides Used Or Unused as DVG Breakpoints

Start and stop positions of DVGs bearing deletions of at least 10 nucleotides and generated in Vero cells were matched with SHAPE reactivity values. Nucleotides that were used as breakpoints or left unused were plotted according to their SHAPE reactivity value. T-test with Sidak's multiple comparisons test was used to compare means.

2.9.4. Comparison of DGVs Generated in WT and D2S Mutant

From the list of deletions generated as described in previous section, we selected the DVG lacking at least 20 nucleotides. We pooled all replicates and passages together for a given virus (WT or D2S mutant; see below). We separated all DVGs in two groups depending of if their start breakpoints were located before or after position 5000. Then, we compared the number of samples containing a given deletion (exact same start and stop position) between WT and mutant, either on a 2D plot or by displaying the distribution of their absolute differences.

2.9.5. DVG Entropy

From the DVG list generated as described above, we calculated an equivalent of Shannon entropy for deletions for each sample as $-\Sigma$ pi log2(pi) where pi is the ratio of the number of reads supporting the junction i over the total number of reads supporting all junctions.

2.9.6. Statistical Analysis

Statistics were performed using R version 4.2.1 (CRAN) or Prism version 8 (Graphpad). All tests were two sided and a p value < 0.05 was considered significant. Correction for multiple testing was performed using Bonferroni's or Sidak's method.

3. Results

3.1. Preferential Generation of DVG Breakpoints at Unpaired Nucleotides

Because DVGs highjack the machinery of full-length virus for replication and/or transmission, they preferentially accumulate at high multiplicity of infection (MOI), when each cell is co-infected with multiple viral particles (Von Magnus 1954; Von Magnus et Gard, 1947). To enrich for DVGs, we performed serial passages at high MOI in triplicates in Vero cells (Fig. S1A). At each passage, half of the supernatant was used to infect cells for the next passage and half was used for next generation sequencing and bioinformatic analysis using an in-house pipeline (Poirier et al. 2018; Levi et al. 2021; Rezelj et al. 2021). DVGs were defined by their start and stop breakpoints corresponding to the first and the last nucleotide deleted (Poirier et al. 2018; Levi et al. 2021; Rezelj et al. 2021) (Fig. 1A, conjointly termed breakpoint nucleotides hereafter). As described in a previous work (Levi et al. 2021), classifying DVGs using their start and the stop position of the truncation identifies clusters of DVGs on the genome (see clusters A, B and C in Figure 1A and B).

We observed no obvious sequence homology between the start and stop regions for the commonly deleted regions, which would suggest template switching to a near homologous region. Additionally, there are currently no reported RNA binding proteins to these regions that would bring the start and stop regions in close proximity during replication allowing the RdRp to skip over the deleted nucleotides. Therefore, we hypothesized that RNA secondary structure in breakpoint regions may play a role in generating these specific DVGs.

We used data generated from our prior SHAPE-MaP analysis of the CHIKV genomic RNA (Madden et al. 2020) to determine the RNA secondary structure of the viral genome around the

 doi:10.20944/preprints202407.1212.v1

breakpoints. Reactive nucleotides, or nucleotides that are more flexible, are colored in orange, while unreactive nucleotides, those that were protected from chemical modification due to base pairing, are colored black in the example region of cluster A and B start breakpoint (nucleotide 300 to 819, Fig 1C). To determine if there was a relationship between a specific nucleotide used as a DVG break site in CHIKV and the flexibility of that nucleotide, we assessed if SHAPE reactivity of breakpoint nucleotides differed from SHAPE reactivity of unused nucleotides after 1 passage in Vero cells (Figure 1D). A median SHAPE reactivity over a 5-nucleotide window was used to capture the flexibility of a hyper-local region around the breakpoint. The average median SHAPE reactivity of nucleotides used as breakpoints remains higher than those not used as breakpoints over all passages, assuming each breakpoint was once originally generated from a full-length genome (Figure S1B).

Next, we analyzed the correlation between the frequency at which a nucleotide was used as a breakpoint (number of reads with this nucleotide as a breakpoint over the total number of reads) with the nucleotide's median SHAPE reactivity (i.e. its probability to be paired when low or unpaired when high, Figure 1C) using a 5-nucleotide window. We used pooled data generated from all replicates over 8 passages (Figure 1E) and focused our analysis on DVGs presenting a deletion of at least 10 nucleotides to exclude all small deletions that might be generated by a short slippage of the viral polymerase rather than a canonical event of non-homologous recombination of RNA molecules. We uncovered an enrichment of unpaired nucleotides in those used as DVG breakpoints even though the relationship is weak (Figure 1E, Pearson correlation r = 0,066, p = 2,7. 10-11).

Together, these results suggest that CHIKV DVG breakpoints preferentially occur at more flexible nucleotides more likely to be unpaired, although flexibility alone is not sufficient to predict a breaksite.

Preprints.org (www.preprints.org) | NOT PEER-REVIEWED | Posted: 15 July 2024 doi:10.20944/preprints202407.1212.v1

Figure 1: CHIKV genome secondary structures correlates with DVG generation

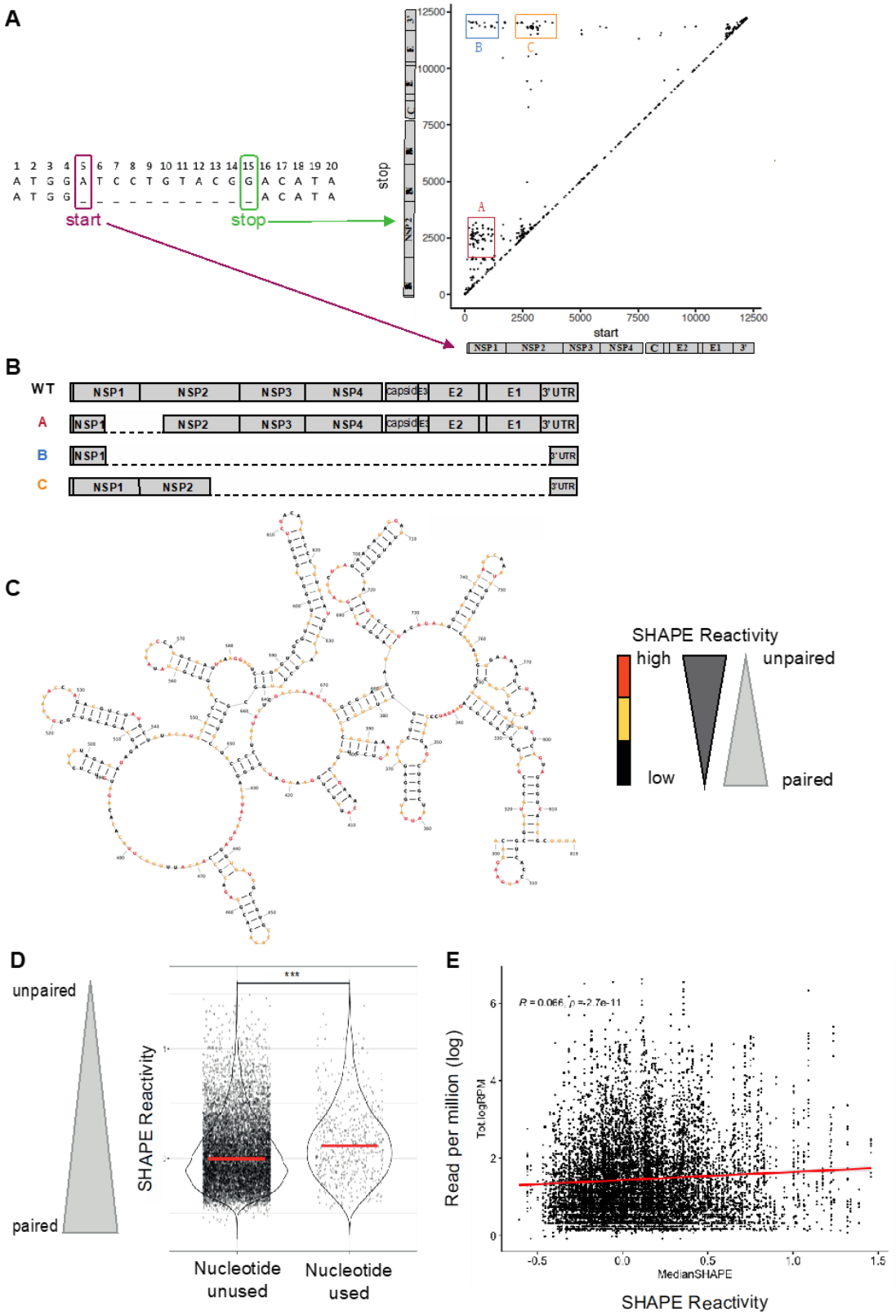

Figure 1. CHIKV genome secondary structures correlates with DVG generation.A, Schematic of start and stop breakpoints of DVGs generated by high MOI passages of CHIKV in Vero cells. Start (x axis) and stop (y axis) positions of the breakpoint of DVGs are plotted. The different clusters are called A, B, and C.B, Schematic of WT CHIKV genome.C, CHIKV Carib secondary structures from the SHAPE-MaP analysis (Madden et al, JVI, 2020) around DVGs A and B start breakpoints (Nucleotide 300 to

 doi:10.20944/preprints202407.1212.v1

819). Nucleotide are depicted in Black (low), red (high) or yellow (intermediate) depending on their SHAPE reactivity.D, In first passage, nucleotides that were used as breakpoints (start and/or stop) or left unused were plotted according to their median SHAPE reactivity value around a 5-nucleotide interval. ***p < 0,001 (unpaired t-test).E, Reads per million values for each nucleotide position used as a start and/or stop breakpoints (start or stop) matched with their respective rolling median SHAPE reactivity (of a 5-nucleotide window) over all passages. r and p denote Pearson's correlation coefficient and its associated p-value.

3.2. CHIKV-D2S Mutant with Disrupted Secondary Structure Is Viable in Cell Culture

To experimentally test the impact of secondary structure on the generation of DVGs, we generated a mutant with disrupted secondary structure (D2S) around a subset of important DVG breakpoints found in CHIKV passages in Vero cells (Figure 1A and Figure 2). We designed D2S mutant so that its secondary structure would be disrupted around DVG breakpoints of clusters A, B and C (all located in the first half of the genome, before nucleotide 5000) without impacting the secondary structure located after nucleotide 5000 (Figure 2A). Hence, we modified 3 regions with a total of 76 synonymous mutations generated using the program CodonShuffle with the dn231 algorithm (Jorge, Mills, et Lauring 2015): 19 mutations were introduced in the first region covering nucleotide 380 to 730 (where cluster A and B start breakpoints are located), 35 mutations between nucleotide 2810 and 3190 (comprising cluster A stop breakpoints and cluster C start breakpoints) and 22 mutations between nucleotide 3800 and 3950 (comprising cluster C stop breakpoints) (Figure 2A and B, list of mutation is depicted in Table S1). The mutations were selected to modify the predicted RNA structure as much as possible without changing amino acid sequence and codon usage (Figure 2B). To assess whether D2S showed decreased fitness (i.e., slower replication kinetics) in these settings compared to WT virus, we performed one-step and multi-step growth curve analyses in Vero cells. The D2S mutant displayed slower growth kinetics with a ten-fold disadvantage compared to WT ($p < 0,0001$; Figure 2C). However, in the one-step growth curve, at 48 hours post-infection, D2S and WT had similar titers in Vero cells. Of note, both Sanger sequencing and deep sequencing results confirmed that none of the mutations introduced in D2S reverted throughout the passages series (data not shown).

Preprints.org (www.preprints.org) | NOT PEER-REVIEWED | Posted: 15 July 2024 doi:10.20944/preprints202407.1212.v1

Figure 2: Engineering a mutant with disrupted secondary structure around breakpoints of clusters A, B and C.

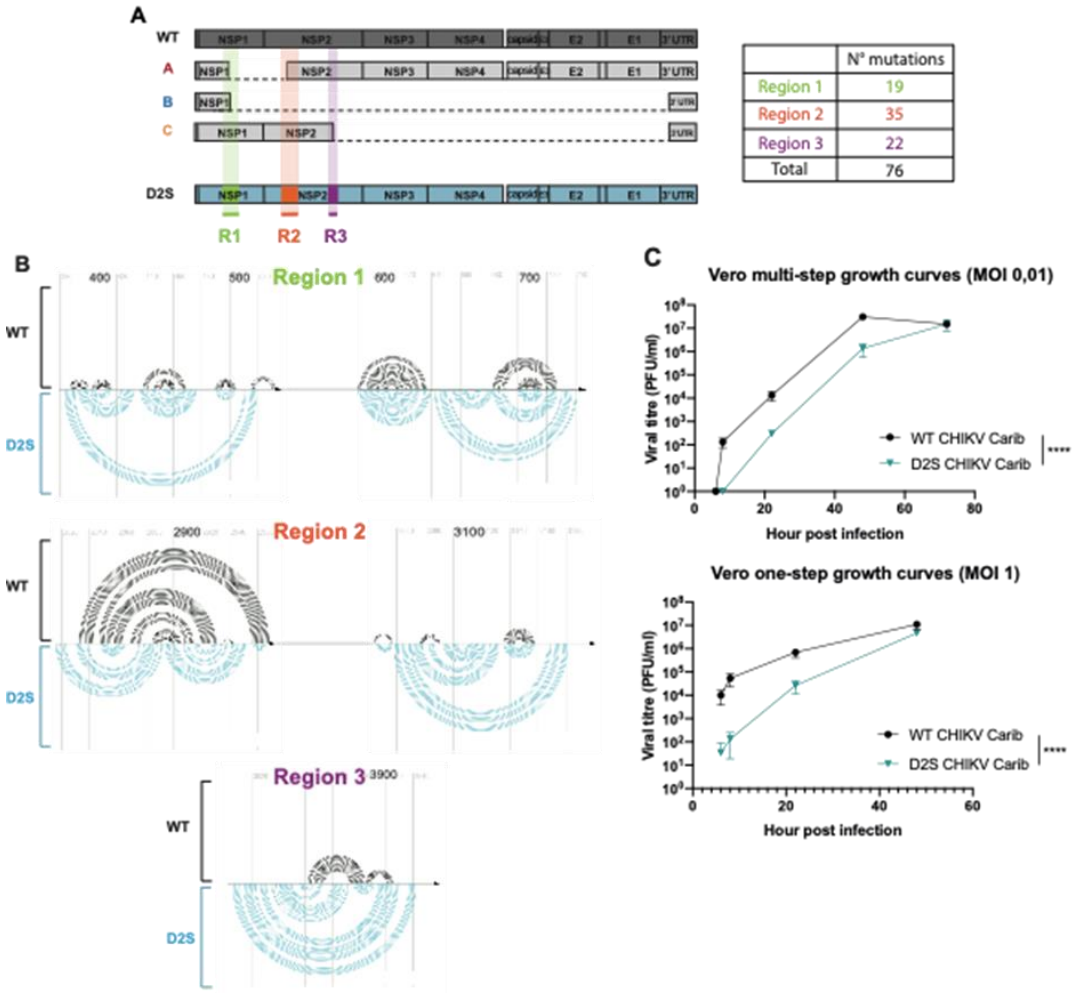

Figure 2. Engineering a mutant with disrupted secondary structure around breakpoints of clusters A, B and C. A, Schematic of WT CHIKV, DVGs from cluster A, B and C and D2S mutant, with highlight on the 3 mutated regions and the number of silent mutations inserted. B, Predicted secondary structures, determined using SHAPE-MaP data for WT virus (black lines) or mFold software for D2S (blue lines) after introducing mutations around regions 1, 2 and 3. The black arrows represent CHIKV genome parts, and each line represents an interaction between 2 nucleotides. Several lines forming an arc form a hairpin. C, Growth curves of D2S CHIKV (blue line) and WT CHIKV (black line) at MOI 0. 01 (multi-step growth curve) and 1 (one-step growth curve) in Vero cells. Bars represent mean ± SD, n = 3 biological replicates; ****p < 0,0001 (two-way ANOVA with Bonferroni post-test).

3.3. Altered DVG Generation in CHIKV D2S Compared to WT Virus

To interrogate the role of genomic RNA secondary structures in the generation of DVGs, we compared the generation of DVGs between WT CHIKV and D2S mutant after high MOI passaging (Figure S1). DVG sequences were characterized by next generation sequencing and visualized depending on their start and stop position. WT and D2S tended to have close global distribution of deletions (Figure 3A). This finding was confirmed by mapping the probability of each nucleotide position to be deleted (Figure S2). To explore the diversity of DVGs generated by wild type and mutant virus, we calculated the equivalent of a Shannon entropy for DVG breakpoints. For both WT and D2S mutant, entropy decreased through passages, suggesting a decrease in DVG diversity over time. Entropy was significantly higher in D2S mutant compared to WT through passages ($p < 0.001$, Figure 3B), illustrating that the D2S mutant generated a more diverse pool of DVGs compared to WT virus.

 doi:10.20944/preprints202407.1212.v1

Figure 3: D2S mutant generates a greater diversity of DVGs.

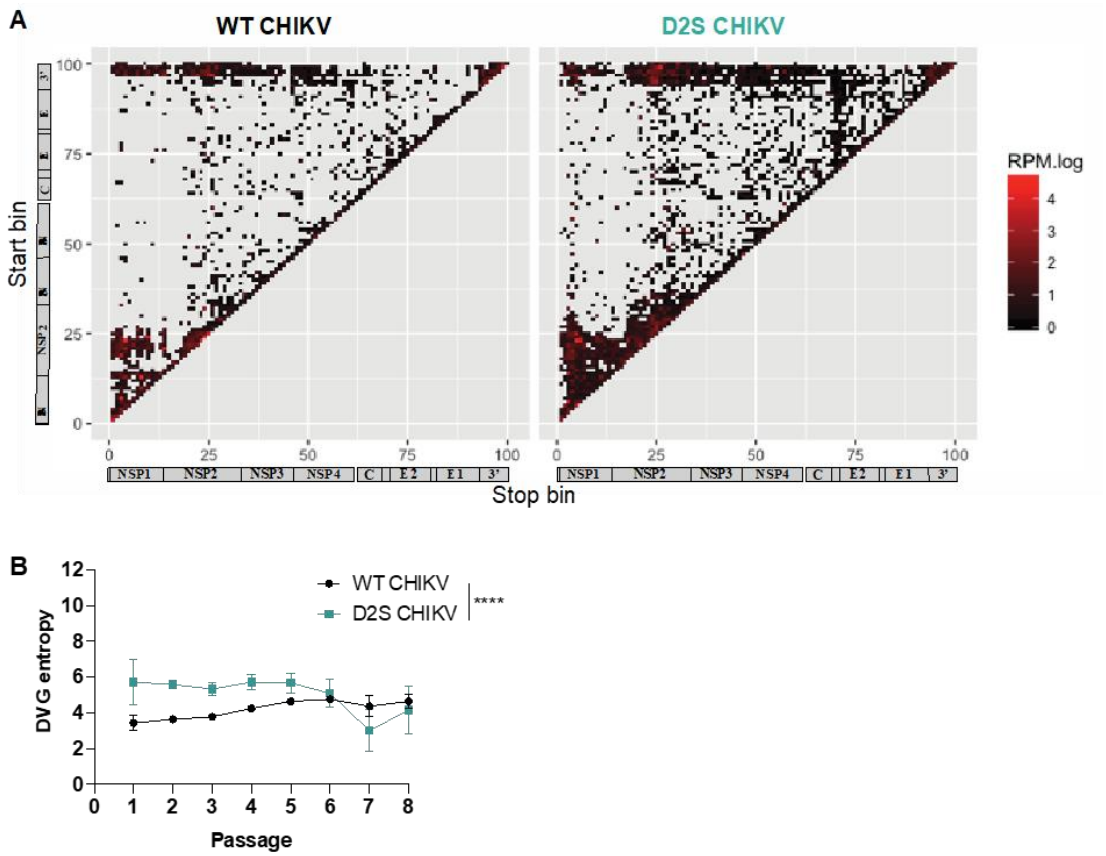

Figure 3. D2S mutant generates a greater diversity of DVGs.A, DVGs were mapped on their start and stop position with colors representing summed frequencies of the DVGs with same start and stop bins. B, DVG entropy of WT and D2S mutant over serial passaging. ****p < 0,001 (unpaired t-test).

3.4. DVG Generation Is Governed by RNA Secondary Structures

To formally evaluate the importance of secondary structure in DVG generation, we separated DVGs depending on their sequence. A first group was made with DVGs showing a start breakpoint before nucleotide 5000, a second group with start breakpoint after nucleotide 5000. The region before 5000 contains the three regions where we disrupted secondary structures, as well as the start breakpoints of the DVG clusters A, B and C, which are predominant in Vero cells (Figure 1A, Figure S2). On the contrary, the region after nucleotide 5000 should display RNA secondary structures equal or similar to WT since no mutations had been introduced there (Figure 1A). We listed all the different deletions present in WT and D2S samples and plotted the number of samples that displayed each individual deletion in WT (x axis) or D2S (y axis). DVGs that appeared predominantly, or only, in one virus would stack along the x and y axes, while DVGs that were common between WT and D2S samples would appear closer to or along the diagonal. We found that DVGs before nucleotide 5000 are often found only in one virus and not the other (Figure 4A), while DVG landscapes were more similar between the two viruses after nucleotide 5000.

To precisely assess this difference in DVG landscape between the two viruses in these regions, we computed, for each specific deletion, the absolute difference between the number of samples supporting these breakpoints in the WT and the DS2 viruses. Then, we computed the number of specific DVGs supporting a specific absolute count difference (Figure 4B). The distributions of these differences significantly differed between DVGs before and after nucleotide 5000, with less similar DVGs (between WT and DS2 mutants) in the first part than in the second part of the genome ($p < 0.0001$, Kolmogorov Smirnov test and unpaired t-test).

 doi:10.20944/preprints202407.1212.v1

We then performed SHAPE-MaP analysis on the D2S mutant to confirm our mutations disrupted the secondary structure of the virus as predicted. We calculated the change in SHAPE at each nucleotide between WT and D2S. If the mutations disrupted local secondary structure, but maintained RNA secondary structure of distal genome regions, there should be a larger change in SHAPE between WT and D2S in and near mutated regions than distal regions. Indeed, the median change in SHAPE reactivity for nucleotides outside the modified regions was significantly smaller than for nucleotides within the modified region, corroborating the interest of the D2S mutant in this experiment (Figure 4C). Then, we looked at SHAPE reactivity values of nucleotides used as breakpoints, with the frequency of their use, and observed a significant correlation ($r = 0.053$, $p = 6.9 \times 10–10$, Figure 4D), as already seen with WT (Figure 1E). Interestingly, this correlation was not significant when using WT SHAPE reactivity values (data not shown) as a reference for D2S DVGs, reinforcing our observations. In line with what was observed with WT, the nucleotides used as breakpoints during D2S infection after a single passage had higher median SHAPE reactivity than nucleotides that were never used as breakpoints (Figure 1E). Together, these data suggest that in both D2S mutant and WT virus, secondary structures influence DVG generation through non-homologous recombination.

Preprints.org (www.preprints.org) | NOT PEER-REVIEWED | Posted: 15 July 2024 doi:10.20944/preprints202407.1212.v1

Figure 4: DVG generation is governed by secondary structures.

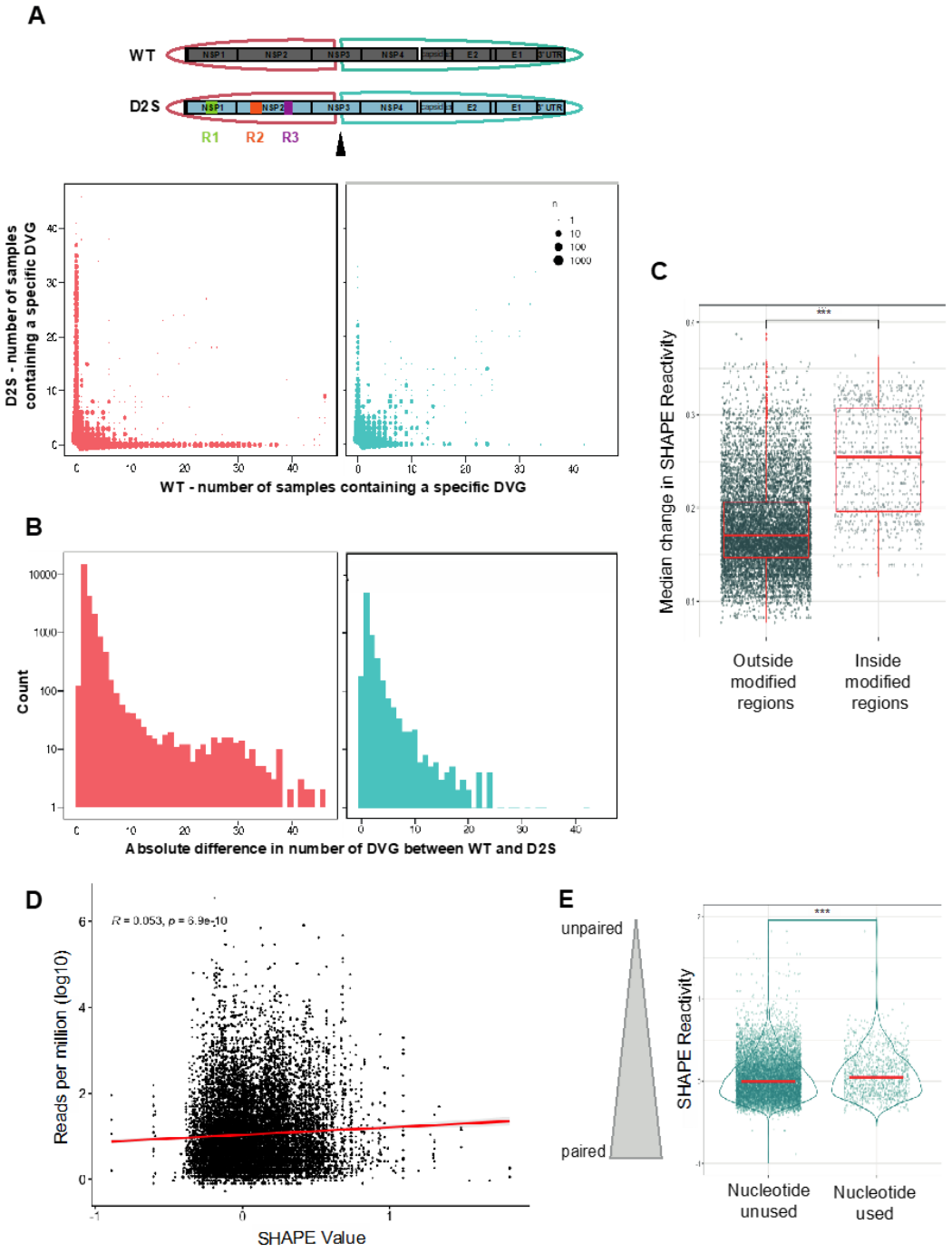

Figure 4. DVG generation is governed by secondary structures.A, All DVG (start, stop) positions pairs found in WT and D2S were listed and associated with the number of DVGs supporting this pair for each virus over all replicates. We separated DVGs that had a start position before (red) and after (blue) the 5000th nucleotide.B, Distribution of the absolute difference between DVG counts in WT vs DS2 viruses for each (start, stop) pair. $p < 0.0001$ (Kolmogorov–Smirnov test and unpaired t-test).C, Median change in SHAPE reactivity of the D2S mutant compared to WT, inside or outside modified regions (R1, R2 and R3 pooled together), ***$p < 0.001$ (unpaired t-test)D, Reads per million values for each nucleotide position used as a start and/or stop breakpoints were matched with its SHAPE reactivity value. r and p denote Pearson's correlation coefficient and its associated p-value.

 doi:10.20944/preprints202407.1212.v1

4. Discussion

Advances in next-generation sequencing technologies allows a more thorough exploration of viral RNA secondary structures: it is already known that RNA secondary structures are key for genome replication and translation in alphaviruses (Kutchko et al. 2018; Madden et al. 2020; Frolov et al. 2001; Niesters et Strauss 1990; Firth et al. 2008; Kendra et al. 2017; 2018; Firth et al. 2011), or in splicing and viral gene expression in HIV (Tomezsko et al. 2020). RNA secondary structures have also been described as being mediators of homologous recombination (Galetto et al. 2004; Simon-Loriere et al. 2010; Baird et al. 2006; Simon-Loriere et Holmes 2011). Concomitantly, DVGs have gathered greater interest over the last decade for their potential use as antiviral molecules (Rezelj et al. 2018; Vignuzzi et López 2019), yet the rules governing their generation are still unclear. Our work supports the notion that RNA secondary structures influence how CHIKV DVGs are generated.

To examine this association, we used RNA secondary structures modeled using SHAPE-MaP analyses of CHIKV genome, which is, to date, the most precise prediction of RNA structures currently attainable(Madden et al. 2020). One of the specificity of our analysis lies in using the median SHAPE reactivity of a 5-nucleotide region around the nucleotide of interest, while studies of SHAPE reactivity generally rely on using the median SHAPE reactivity of a 50-nucleotide window (Kutchko et al. 2018; Smola et al. 2015; Huber et al. 2019). Indeed, although DVG recombination sites can occur in highly structured regions, it could preferentially happen on the unpaired, rather than paired, nucleotides of such secondary structures. We chose to exclude the 3'UTR region from analysis, even though CHIKV DVGs breakpoints often occur in this region (Levi et al. 2021): many sequence repeats complicate the analysis and decrease prediction performance compared to genomic RNA (Marinus et al. 2021). Finally, our initial analyses pooled DVGs from all passages combined, which makes it impossible to differentiate newly generated DVGs from DVGs that are replicated from a previous DVG template.

The reported correlation between DVG breakpoint probability and SHAPE reactivity, although significant, remains moderate. Our data therefore suggest that if RNA structure is an important driver of DVG formation, it remains complex and coupled to other determinants. This finding is consistent with what was observed in our previous work on CHIKV DVGs (Levi et al. 2021): DVGs can be produced in various species, but their sequence and abundance depend on both cellular environment and the viral genome. Other determinants may include RNA–cellular or RNA–viral protein interactions, long distance RNA interactions (tertiary structures or interaction with cellular RNA), sequence homology around breakpoints, cellular ionic concentrations, innate immunity pressure, or location of viral replication.

We were able to experimentally test the putative role of secondary structure in DVG formation by creating a mutant with altered secondary structure. To our knowledge, only two studies have disrupted secondary structures of alphaviruses at the nucleotide level without modifying the amino-acid sequence using CodonShuffle (Jorge et al. 2015). Using SINV and CHIKV, the authors introduced mutations in the RNA secondary structures and confirmed that these mutants had growth defects, therefore arguing for the importance of secondary structures in these regions (Kutchko et al. 2018; Madden et al. 2020). One pitfall of this method, is the absence of controls bearing the same number of mutations without disrupting the secondary structure that would behave as WT. In our case, because any slight nucleotide change could cause recombination changes in the hypothetical DVG breakpoints being shaped by the RNA structures, it is close to impossible to design such a control. Nevertheless, this drawback was compensated by the fact that we split the genome in two: a first region before the 5000th nucleotide where the RNA secondary structure was greatly disrupted and a second region after nucleotide 5000 where secondary structure was similar to WT, providing some internal control. Notwithstanding, because disrupting secondary structures could also impact long distance interactions (tertiary structures) or protein interactions, recombination areas could still be affected in the second half of the genome, which may explain the remaining differences between DS2 and WT DVG landscapes in this unchanged region.

Even though DVGs with large deletions generated from WT and D2S mutants do not present the exact same breakpoints, both viruses tend to delete the same regions when passaged in the same

cell type. However, D2S mutant seems to fumble when generating DVGs: it creates more diverse DVGs, at lower frequencies. Environmental pressure may still drive a particular kind of DVG, while the abnormal secondary structure makes it harder to select for specific DVGs. This may imply that the WT genome has evolved to maintain or avoid the generation of certain DVGs.

In conclusion, although other determinants are involved, RNA secondary structures do drive CHIKV DVG formation. Further work is needed to narrow down which specific RNA structures are involved in DVG generation, and to pinpoint other determinants such as sequence homology around breakpoints, RNA protein interaction or RNA tertiary structures. A broader knowledge of these mechanisms could help develop prediction tools for DVG generation in different viruses and to better genetically engineer genomes and DVGs for therapeutic purposes.

Author Contributions: L.I.L and E.M conceptualized the work and performed experiments and analyses. W.S. preformed SHAPE-MaP experiment. L.I.L, E.M., J.B., D.E., V.B., W.S., N.J.M. performed bioinformatics analyses. M.H. and M.V. supervised and acquired funding. L.I.L, J.B. and E.Z.P. wrote the initial manuscript. All authors reviewed and edited the manuscript.

Acknowledgments: This work was supported by a grant from the DARPA INTERCEPT program administered though DARPA Cooperative Agreement #HR0011-17-2-0023 to M.V. L.I.L. was funded by a doctoral fellowship from France's defence procurement agency (DGA). The work was supported by NIH Grant R21 AI138056 to MH and NJM. E.M. received support from T32AI007419-26. LIL thanks Lucia Carrau and Enzo Poirier for scientific discussions.

Conflicts of Interest: L.I.L., V.B, T.V. and M.V. are co-inventors of the DI 2018-21 patent. The rest of the authors declare no conflict of interest. None of the funders described below had any influence on study design, data collection and analysis, decision to publish, or preparation of the manuscript.

References

Baird, Heather A., Román Galetto, Yong Gao, Etienne Simon-Loriere, Measho Abreha, John Archer, Jun Fan, David L. Robertson, Eric J. Arts, et Matteo Negroni. 2006. « Sequence Determinants of Breakpoint Location during HIV-1 Intersubtype Recombination ». Nucleic Acids Research 34 (18): 5203-16. https://doi.org/10.1093/nar/gkl669.

Borgherini, Gianandrea, Patrice Poubeau, Annie Jossaume, Arnaud Gouix, Liliane Cotte, Alain Michault, Claude Arvin-Berod, et Fabrice Paganin. 2008. « Persistent Arthralgia Associated with Chikungunya Virus: A Study of 88 Adult Patients on Reunion Island ». Clinical Infectious Diseases 47 (4): 469-75. https://doi.org/10.1086/590003.

Borgherini, Gianandrea, Patrice Poubeau, Frederik Staikowsky, Manuella Lory, Nathalie Le Moullec, Jean Philippe Becquart, Catherine Wengling, Alain Michault, et Fabrice Paganin. 2007. « Outbreak of Chikungunya on Reunion Island: Early Clinical and Laboratory Features in 157 Adult Patients ». Clinical Infectious Diseases 44 (11): 1401-7. https://doi.org/10.1086/517537.

Bouquillard, Eric, Adrian Fianu, Marianne Bangil, Nathalie Charlette, Anne Ribéra, Alain Michault, François Favier, Fabrice Simon, et René-Marc Flipo. 2018. « Rheumatic Manifestations Associated with Chikungunya Virus Infection: A Study of 307 Patients with 32-Month Follow-up (RHUMATOCHIK Study) ». Joint, Bone, Spine: Revue Du Rhumatisme 85 (2): 207-10. https://doi.org/10.1016/j.jbspin.2017.01.014.

Chao, Mei, Tzu-Chi Wang, Chia-Chi Lin, Robert Yung-Liang Wang, Wen-Bin Lin, Shang-En Lee, Ying-Yu Cheng, Chau-Ting Yeh, et Shan-Bei Iang. 2017. « Analyses of a Whole-Genome Inter-Clade Recombination Map of Hepatitis Delta Virus Suggest a Host Polymerase-Driven and Viral RNA Structure-Promoted Template-Switching Mechanism for Viral RNA Recombination ». Oncotarget 8 (37): 60841-59. https://doi.org/10.18632/oncotarget.18339.

Chretien, Jean-Paul, Assaf Anyamba, Sheryl A Bedno, Robert F Breiman, Rosemary Sang, Kibet Sergon, Ann M Powers, et al. 2007. « DROUGHT-ASSOCIATED CHIKUNGUNYA EMERGENCE ALONG COASTAL EAST AFRICA », mars, 3.

Couturier, Elisabeth, Francis Guillemin, Marie Mura, Lucie Léon, Jean-Marc Virion, Marie-José Letort, Henriette De Valk, Fabrice Simon, et Véronique Vaillant. 2012. « Impaired Quality of Life after Chikungunya Virus Infection: A 2-Year Follow-up Study ». Rheumatology 51 (7): 1315-22. https://doi.org/10.1093/rheumatology/kes015.

Dedepsidis, Evaggelos, Zaharoula Kyriakopoulou, Vaia Pliaka, et Panayotis Markoulatos. 2010. « Correlation between Recombination Junctions and RNA Secondary Structure Elements in Poliovirus Sabin Strains ». Virus Genes 41 (2): 181-91. https://doi.org/10.1007/s11262-010-0512-5.

Easton, Andrew J., Paul D. Scott, Nicole L. Edworthy, Bo Meng, Anthony C. Marriott, et Nigel J. Dimmock. 2011. « A Novel Broad-Spectrum Treatment for Respiratory Virus Infections: Influenza-Based Defective Interfering Virus Provides Protection against Pneumovirus Infection in Vivo ». Vaccine 29 (15): 2777-84. https://doi.org/10.1016/j.vaccine.2011.01.102.

Figlerowicz, Marek. 2000. « Role of RNA structure in non-homologous recombination between genomic molecules of brome mosaic virus ». Nucleic Acids Research 28 (8): 1714-23.

Firth, Andrew E., Betty Yw Chung, Marina N. Fleeton, et John F. Atkins. 2008. « Discovery of Frameshifting in Alphavirus 6K Resolves a 20-Year Enigma ». Virology Journal 5 (septembre): 108. https://doi.org/10.1186/1743-422X-5-108.

Firth, Andrew E., Norma M. Wills, Raymond F. Gesteland, et John F. Atkins. 2011. « Stimulation of Stop Codon Readthrough: Frequent Presence of an Extended 3′ RNA Structural Element ». Nucleic Acids Research 39 (15): 6679-91. https://doi.org/10.1093/nar/gkr224.

Frolov, I., R. Hardy, et C. M. Rice. 2001. « Cis-Acting RNA Elements at the 5′ End of Sindbis Virus Genome RNA Regulate Minus- and plus-Strand RNA Synthesis. » RNA 7 (11): 1638-51.

Galetto, Román, Abdeladim Moumen, Véronique Giacomoni, Michel Véron, Pierre Charneau, et Matteo Negroni. 2004. « The Structure of HIV-1 Genomic RNA in the Gp120 Gene Determines a Recombination Hot Spot in Vivo ». The Journal of Biological Chemistry 279 (35): 36625-32. https://doi.org/10.1074/jbc.M405476200.

Havelda, Z, J Burgy√°n, et T Dalmay. 1997. « Secondary Structure-Dependent Evolution of Cymbidium Ringspot Virus Defective Interfering RNA. » Journal of General Virology 78 (6): 1227-34. https://doi.org/10.1099/0022-1317-78-6-1227.

Huber, Roland G., Xin Ni Lim, Wy Ching Ng, Adelene Y. L. Sim, Hui Xian Poh, Yang Shen, Su Ying Lim, et al. 2019. « Structure Mapping of Dengue and Zika Viruses Reveals Functional Long-Range Interactions ». Nature Communications 10 (1): 1408. https://doi.org/10.1038/s41467-019-09391-8.

Jorge, Daniel Macedo de Melo, Ryan E. Mills, et Adam S. Lauring. 2015. « CodonShuffle: A Tool for Generating and Analyzing Synonymously Mutated Sequences ». Virus Evolution 1 (1): vev012. https://doi.org/10.1093/ve/vev012.

Kendra, Joseph A., Vivek M. Advani, Bin Chen, Joseph W. Briggs, Jinyi Zhu, Hannah J. Bress, Sushrut M. Pathy, et Jonathan D. Dinman. 2018. « Functional and Structural Characterization of the Chikungunya Virus Translational Recoding Signals ». Journal of Biological Chemistry 293 (45): 17536-45. https://doi.org/10.1074/jbc.RA118.005606.

Kendra, Joseph A., Cynthia de la Fuente, Ashwini Brahms, Caitlin Woodson, Todd M. Bell, Bin Chen, Yousuf A. Khan, Jonathan L. Jacobs, Kylene Kehn-Hall, et Jonathan D. Dinman. 2017. « Ablation of Programmed -1 Ribosomal Frameshifting in Venezuelan Equine Encephalitis Virus Results in Attenuated Neuropathogenicity ». Journal of Virology 91 (3). https://doi.org/10.1128/JVI.01766-16.

Kutchko, Katrina M, Emily A Madden, Clayton Morrison, Kenneth S Plante, Wes Sanders, Heather A Vincent, Marta C Cruz Cisneros, et al. 2018. « Structural divergence creates new functional features in alphavirus genomes ». Nucleic Acids Research 46 (7): 3657-70. https://doi.org/10.1093/nar/gky012.

Levi, Laura I., Veronica V. Rezelj, Annabelle Henrion-Lacritick, Diana Erazo, J Boussier, Thomas Vallet, Veronika Bernhauerová, et al. 2021. « Defective Viral Genomes from Chikungunya Virus Are Broad-Spectrum Antivirals and Prevent Virus Dissemination in Mosquitoes ». Édité par Adam S. Lauring. PLOS Pathogens 17 (2): e1009110. https://doi.org/10.1371/journal.ppat.1009110.

Levi, Laura I., et Marco Vignuzzi. 2019. « Arthritogenic Alphaviruses: A Worldwide Emerging Threat? » Microorganisms 7 (5): 133. https://doi.org/10.3390/microorganisms7050133.

Low, Justin T., et Kevin M. Weeks. 2010. « SHAPE-Directed RNA Secondary Structure Prediction ». Methods (San Diego, Calif.) 52 (2): 150-58. https://doi.org/10.1016/j.ymeth.2010.06.007.

Madden, Emily A., Kenneth S. Plante, Clayton R. Morrison, Katrina M. Kutchko, Wes Sanders, Kristin M. Long, Sharon Taft-Benz, et al. 2020. « Using SHAPE-MaP To Model RNA Secondary Structure and Identify 3′UTR Variation in Chikungunya Virus ». Édité par Rebecca Ellis Dutch. Journal of Virology 94 (24): e00701-20. https://doi.org/10.1128/JVI.00701-20.

Marcus, P. I., et M. J. Sekellick. 1977. « Defective Interfering Particles with Covalently Linked [+/-]RNA Induce Interferon ». Nature 266 (5605): 815-19. https://doi.org/10.1038/266815a0.

Marinus, Tycho, Adam B Fessler, Craig A Ogle, et Danny Incarnato. 2021. « A Novel SHAPE Reagent Enables the Analysis of RNA Structure in Living Cells with Unprecedented Accuracy ». Nucleic Acids Research 49 (6): e34-e34. https://doi.org/10.1093/nar/gkaa1255.

Merino, Edward J., Kevin A. Wilkinson, Jennifer L. Coughlan, et Kevin M. Weeks. 2005. « RNA Structure Analysis at Single Nucleotide Resolution by Selective 2′-Hydroxyl Acylation and Primer Extension (SHAPE) ». Journal of the American Chemical Society 127 (12): 4223-31. https://doi.org/10.1021/ja043822v.

Monroe, S S, et S Schlesinger. 1984. « Common and Distinct Regions of Defective-Interfering RNAs of Sindbis Virus ». Journal of Virology 49 (3): 865-72. https://doi.org/10.1128/jvi.49.3.865-872.1984.

Moumen, Abdeladim, Lucette Polomack, Torsten Unge, Michel Véron, Henri Buc, et Matteo Negroni. 2003. « Evidence for a Mechanism of Recombination during Reverse Transcription Dependent on the Structure of the Acceptor RNA ». The Journal of Biological Chemistry 278 (18): 15973-82. https://doi.org/10.1074/jbc.M212306200.

Nicholson, Beth L., et K. Andrew White. 2014. « Functional Long-Range RNA-RNA Interactions in Positive-Strand RNA Viruses ». Nature Reviews. Microbiology 12 (7): 493-504. https://doi.org/10.1038/nrmicro3288.

———. 2015. « Exploring the Architecture of Viral RNA Genomes ». Current Opinion in Virology 12 (juin): 66-74. https://doi.org/10.1016/j.coviro.2015.03.018.

Niesters, H. G., et J. H. Strauss. 1990. « Mutagenesis of the Conserved 51-Nucleotide Region of Sindbis Virus ». Journal of Virology 64 (4): 1639-47.

Poirier, Enzo Z., Bertsy Goic, Lorena Tomé-Poderti, Lionel Frangeul, Jérémy Boussier, Valérie Gausson, Hervé Blanc, et al. 2018. « Dicer-2-Dependent Generation of Viral DNA from Defective Genomes of RNA Viruses Modulates Antiviral Immunity in Insects ». Cell Host & Microbe 23 (3): 353-365.e8. https://doi.org/10.1016/j.chom.2018.02.001.

Rausch, Jason W., Joanna Sztuba-Solinska, et Stuart F. J. Le Grice. 2017. « Probing the Structures of Viral RNA Regulatory Elements with SHAPE and Related Methodologies ». Frontiers in Microbiology 8: 2634. https://doi.org/10.3389/fmicb.2017.02634.

Rezelj, Veronica V., Lucía Carrau, Fernando Merwaiss, Laura I. Levi, Diana Erazo, Quang Dinh Tran, Annabelle Henrion-Lacritick, et al. 2021. « Defective Viral Genomes as Therapeutic Interfering Particles against Flavivirus Infection in Mammalian and Mosquito Hosts ». Nature Communications 12 (1): 2290. https://doi.org/10.1038/s41467-021-22341-7.

Rezelj, Veronica V, Laura I Levi, et Marco Vignuzzi. 2018. « The Defective Component of Viral Populations ». Current Opinion in Virology 33 (décembre): 74-80. https://doi.org/10.1016/j.coviro.2018.07.014.

Siegfried, Nathan A., Steven Busan, Greggory M. Rice, Julie A. E. Nelson, et Kevin M. Weeks. 2014. « RNA Motif Discovery by SHAPE and Mutational Profiling (SHAPE-MaP) ». Nature Methods 11 (9): 959-65. https://doi.org/10.1038/nmeth.3029.

Simon-Loriere, Etienne, et Edward C. Holmes. 2011. « Why Do RNA Viruses Recombine? » Nature Reviews Microbiology 9 (8): 617-26. https://doi.org/10.1038/nrmicro2614.

Simon-Loriere, Etienne, Darren P. Martin, Kevin M. Weeks, et Matteo Negroni. 2010. « RNA Structures Facilitate Recombination-Mediated Gene Swapping in HIV-1 ». Journal of Virology 84 (24): 12675-82. https://doi.org/10.1128/JVI.01302-10.

Smola, Matthew J., Greggory M. Rice, Steven Busan, Nathan A. Siegfried, et Kevin M. Weeks. 2015. « Selective 2′-Hydroxyl Acylation Analyzed by Primer Extension and Mutational Profiling (SHAPE-MaP) for Direct, Versatile and Accurate RNA Structure Analysis ». Nature Protocols 10 (11): 1643-69. https://doi.org/10.1038/nprot.2015.103.

Stapleford, Kenneth A., Gonzalo Moratorio, Rasmus Henningsson, Rubing Chen, Séverine Matheus, Antoine Enfissi, Daphna Weissglas-Volkov, et al. 2016. « Whole-Genome Sequencing Analysis from the Chikungunya Virus Caribbean Outbreak Reveals Novel Evolutionary Genomic Elements ». PLoS Neglected Tropical Diseases 10 (1): e0004402. https://doi.org/10.1371/journal.pntd.0004402.

Suhrbier, Andreas, Marie-Christine Jaffar-Bandjee, et Philippe Gasque. 2012. « Arthritogenic Alphaviruses--an Overview ». Nature Reviews. Rheumatology 8 (7): 420-29. https://doi.org/10.1038/nrrheum.2012.64.

Sun, Yan, Deepika Jain, Cynthia J. Koziol-White, Emmanuelle Genoyer, Micah Gilbert, Karla Tapia, Reynold A. Panettieri, Richard L. Hodinka, et Carolina B. López. 2015. « Immunostimulatory Defective Viral Genomes from Respiratory Syncytial Virus Promote a Strong Innate Antiviral Response during Infection in Mice and Humans ». Édité par Paul G. Thomas. PLOS Pathogens 11 (9): e1005122. https://doi.org/10.1371/journal.ppat.1005122.

Tomezsko, Phillip J., Vincent D. A. Corbin, Paromita Gupta, Harish Swaminathan, Margalit Glasgow, Sitara Persad, Matthew D. Edwards, et al. 2020. « Determination of RNA Structural Diversity and Its Role in HIV-1 RNA Splicing ». Nature 582 (7812): 438-42. https://doi.org/10.1038/s41586-020-2253-5.

Vasilijevic, Jasmina, Noelia Zamarreño, Juan Carlos Oliveros, Ariel Rodriguez-Frandsen, Guillermo Gómez, Guadalupe Rodriguez, Mercedes Pérez-Ruiz, et al. 2017. « Reduced Accumulation of Defective Viral Genomes Contributes to Severe Outcome in Influenza Virus Infected Patients ». Édité par Paul G. Thomas. PLOS Pathogens 13 (10): e1006650. https://doi.org/10.1371/journal.ppat.1006650.

Vignuzzi, Marco, et Stephen Higgs. 2017. « The Bridges and Blockades to Evolutionary Convergence on the Road to Predicting Chikungunya Virus Evolution ». Annual Review of Virology 4 (1): 181-200. https://doi.org/10.1146/annurev-virology-101416-041757.

Vignuzzi, Marco, et Carolina B. López. 2019. « Defective Viral Genomes Are Key Drivers of the Virus–Host Interaction ». Nature Microbiology, juin, 1. https://doi.org/10.1038/s41564-019-0465-y.

Von Magnus, P. 1954. « Incomplete Forms of Influenza Virus ». Advances in Virus Research 2: 59-79.

Von Magnus, P, et S Gard. s. d. « Studies on interference in experimental influenza ». Arkiv för kemi, mineralogi och geologi 24 (1). https://books.google.fr/books/about/Studies_on_interference_in_experimental.html?id=f-IEHQAACAAJ&redir_esc=y.

Wang, Haiwei, Xingyang Cui, Xuehui Cai, et Tongqing An. 2022. « Recombination in Positive-Strand RNA Viruses ». Frontiers in Microbiology 13 (mai): 870759. https://doi.org/10.3389/fmicb.2022.870759.

Wilkinson, Kevin A., Edward J. Merino, et Kevin M. Weeks. 2006. « Selective 2′-Hydroxyl Acylation Analyzed by Primer Extension (SHAPE): Quantitative RNA Structure Analysis at Single Nucleotide Resolution ». Nature Protocols 1 (3): 1610-16. https://doi.org/10.1038/nprot.2006.249.

 doi:10.20944/preprints202407.1212.v1

disclaim responsibility for any injury to people or property resulting from any ideas, methods, instructions or products referred to in the content.